JSEE Vol. 23, No. 1, 2021 DOI: 10.48303/jsee.2022.563581.1031

Research Paper

Land Surface Deformation in the 2022 March 16 Kookhord-Bastak Earthquake (Mw6): Using Radar Interferometry Technique

Fateme Kamalia[1], Mohammad Mohammadhasani[2], Mobin Bahrampur[3], and Ahmad Rashidi[4*]

1. M.A. Student in Remote Sensing and Geographic Information System: Majoring in Remote Sensing, Department of Geography, Yazd National University, Yazd, Iran
2. Academic Member of Building, Housing and road Research Center (BHRC), Tehran, Iran
3. M.A. Student in Geography and Urban Planning, Department of Geography, Shahid Bahonar University of Kerman, Kerman, Iran
4. Assistant Professor, Seismological Research Center, International Institute of Earthquake Engineering and Seismology, Tehran, Iran,
*Corresponding Author; email: rashidi@iiees.ac.ir

Received: 16/10/2022
Revised: 26/11/2022
Accepted: 20/12/2022

ABSTRACT

Earthquakes are one of the most important environmental hazards, which have usually been associated with the human and financial damages. In addition to its effects on residential areas, earthquake causes displacements and changes in the ground's surface. Iranian plate is located in the convergence zone of the Arabian plate in the southwest and the Eurasian plate in the northeast; therefore, it is a tectonically unstable area. The earth's deformation and the subsidence resulting from the destructive earthquake occurrence have been as the most important natural hazards in this plate. Several methods are used to study the effects of natural hazards on the land and settlements. Radar interference technique is one of the practical methods in investigating and measuring the amount of displacement. In recent years, many space sensors have been collecting data from the surface of the earth, one of the most successful of which is the Sentinel project. Sentinel-1 is the radar section of the Sentinel project, which captures images of the Earth's surface at intervals of several days and is therefore suitable for monitoring surface changes and estimating the amount of earth movement using the radar interferometry method. In this article, the deformation related to the March 16, 2022 Kookhord-Bastak earthquake (Mw6) in the Hormozgan province is measured. The results show 19 cm of subsidence and 14 cm of uplift along the fault plane and around area during the earthquake.

Keywords:
Radar Interferometry; Sentinel One; Earthquake Deformation; Kookhord-Bastak Earthquake; Hormozgan; Iran

1. Introduction

Earthquakes are natural phenomena that can occur at any time on the ground surface [1-2]. Major earthquakes are among the most devastating natural disasters that often lead to massive fatalities and destruction [3-7]. The technique of interferometry (InSAR) is able to measure the deformation of the ground surface during the earthquakes [8-10]).

The InSAR images carry phase information with measuring signal strength. Using phase information and InSAR interferometry method, the images are used in the fault and earthquake studies [11-13]. Radar interferometry method for precise landslide control has become very common in the past decade [14-15].

The technique of interferometry (InSAR) was first used by Gabriel et al. [16] using three images. This technology makes it possible to detect very small changes on a daily scale [17]. Insar remote sensing technique is capable of working in all weather conditions. With its extensive land cover and high temporal and spatial resolution, it is one of the most accurate and cost-effective remote sensing techniques [16]. The simplest method in this field is to use at least two images obtained from InSAR sensors with artificial apertures in the form of interferometer [18]. With regard to the advances in InSAR interferometry technique, several researches have been done in the field of earthquake displacement detection and monitoring. Some researchers [e.g. 19-20] used InSAR interferometry technique to investigate the cause of the Bam earthquake and concluded that the Bam earthquake was due to the activation of a new fault other than the old Bam fault. Cigna et al. [21] investigated the surface displacement in the Morillia area of Mexico using InSAR interferometry techniques. By analyzing the data, they concluded a displacement of 7-8 cm per year in the direction parallel to the main fault. In 2013, Kaneko et al. [22] measured the seismic deformation in the central part of the Anatolian fault in Turkey using InSAR interferometry techniques. They concluded that this technique has valuable potential in fault studies. Feng et al. [23] studied the Gorkha-Nepal earthquake using satellite imagery of RADARSAT, Sentinel 1 and ALOS-2. They estimated the amount of ground movement using the InSAR interferometry technique, a maximum slip of 6 m at a depth of 13 km. Mohammadhasani et al. [24] studied the subsidence rate in western part of Kerman province using interferometry of InSAR images of sentinel-1 satellite data. They stated the ability of snap software using sentinel-1 satellite data in evaluation of subsidence.

Kandergula et al. [25] investigated the regional surface deformation of the 2001 Bhoj earthquake in Kachchh region in the West of India. In their study, they measured the displacement using radar interferometry, 15 ENVI ASAR images, 6 pairs of ALOS PALSAR satellite images, and 117 images from SENTINEL 1A during three periods: 2003-2005, 2007-2009 and 2016-2020. The results of the PSI method showed that the maximum displacement during the years 2003 to 2005 was equal to 22 mm. Using ALOS POLSAR satellite data, the maximum displacement was equal to 1.2 cm during the years 2007 to 2009. Using the SENTINEL 1A satellite data set, in the period from 2016 to 2020, a maximum displacement of 16 mm per year has occurred in the western region, 6 mm of uplift per year and 8 mm per year in the main area of the eastern Koch. The results showed that the acquired shape change rate is correlated with the results of the spatial information system and the results of this research are reliable.

Syafriani et al. [26] investigated land surface changes in which, by comparing satellite images before and after the earthquake, they found that parts of Padang city had a 40 mm drop in height, and 0-20 mm of precipitation was seen along the coast of Padang city.

In this research, the aim is to estimate the amount of surface displacement caused by the March 16, 2022 Kookhord-Bastak earthquake (Mw6; Depth 10 km) using Sentinel-1 InSAR images and processing them by InSAR interference method (see the location in Figure 1). Kookhord area with an area of about 1600 square km is located in the southeastern part of Bastak city, Hormozgan province in southern Iran. The area is limited from the north to Nakh mountains and the central part of Bastak and Lavar mountains, from the south to Din, Sefid mountains and the central part of Bandar-e Lengeh city, from the west to Khulus desert and Jinnah and from the east to Lamzan village and Pedel.

2. Materials and methods

The research method in the present study is an applied analytical descriptive. To conduct this research, information about the epicenter and location of the Kookhord-Bastak earthquake was obtained from the sites of the IIEES, IRSC and BHRC. Then, two Sentinel-1 radar images, one related to before and another related to after the earthquake, were prepared in the form of a research project from the European Space Agency. The image that is related to before the earthquake is

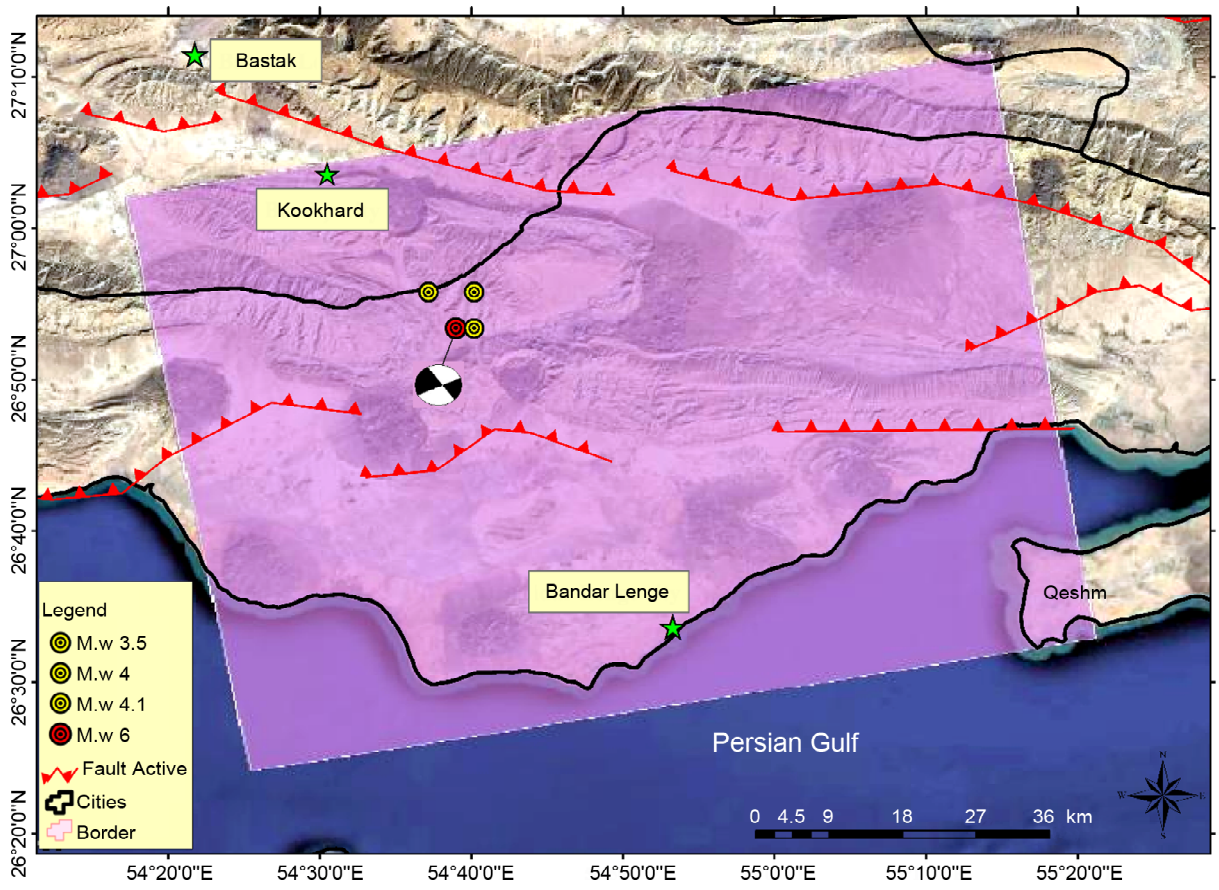

Figure 1. The locations of the March 16, 2022 Kookhord-Bastak earthquake (Mw 6) and three aftershocks (Mw 3.5, 4, 4.1) with the position of the processed Sentinel-1 radar image. Faults modified after Hessami et al. [27].

Figure 1. The characteristic of the processed Sentinel-1 radar image in the Kookhord-Bastak.

Image Number	Shooting Date (day/month/year)	Imaging Format	Shooting Mode	Transit and Polarization Imaging	Polarization	Frame Numbers
1 (base)	03/06/2022	SLC	IW	ISDV	VV	042202
2 (follower)	03/30/2022	SLC	IW	ISDV	VV	042552

called the base image and the other one that is related to the after the earthquake is called the follower image. These images are both shot descending.

The used images in this study were tried to have a minimum baseline (distance between satellite flight paths) (Table 1), because in the interferometry technique, the ground's surface displacement displayed better when the spatial base distance of the data are shorter.

Interferometry processes and techniques were performed by the snap software, the steps of which are shown in Figure (2).

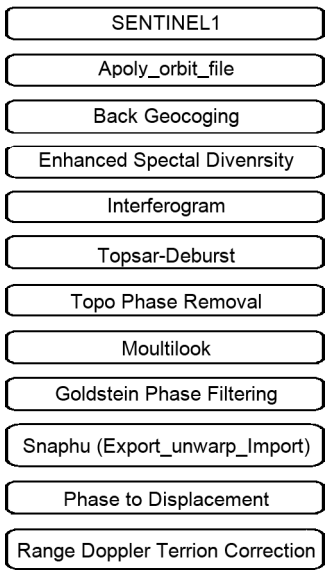

Figure 2. Flowchart of different steps of calculating the displacement map of the ground surface using Sentinel-1 image.

3. Radar Interference

According to Gabriel et al. [16], differential radar interferometry can achieve an accuracy of

~1 cm or even better, which means that this method can be used to accurately measure geophysical phenomena, earthquakes and volcanoes [17]. The used images are obtained by special antennas mounted on satellites or airplanes and show changes in the earth's crust. Interference of images is obtained by multiplying the first image (base image) in the conjugate of the second image (follower image). The interference phase of the product is multi-component topographic mapping, shell displacement signal, atmospheric component effect, orbital component effect and noise, which can be seen in Equation 1:

$$\partial\varnothing = \partial\varnothing topo + \partial\varnothing disp + \partial\varnothing atm + \partial\varnothing orb + \partial\varnothing nois \quad (1)$$

According to the equation, the work process is such that the effect of the orbit is reduced using orbital parameters, the effect of the atmosphere in arid areas is considered zero, the effect of the topography of the earth was removed from the image using DEM SRTM. By removing all these effects, a mapping image is obtained, and each cycle of this image represents the displacement of the earth's crust. In the present study, in order to calculate the amount of crustal displacement during the March 16, 2022 Kookhord-Bastak earthquake (Mw6), the processing results can be seen in the following sections.

4. Results and Discussion

Two Sentinel-1 radar images were taken, one before the Kookhord-Bastak earthquake and the other after the earthquake, so that it can show the effects of the earthquake on the ground surface as a displacement phase. For this purpose, using the base and follower images, interference image was prepared. As can be seen in Figure (3), a series of fringes have been created around the earthquake site in the interference map. The amount of movement in the direction of satellite view is obtained by counting the number of fringes. Depending on the position of the observed color cycle, the amount of displacement are also varies. If the color cycle is yellow, orange, and purple, the off-radar shift occurs, and if the color cycle is green,

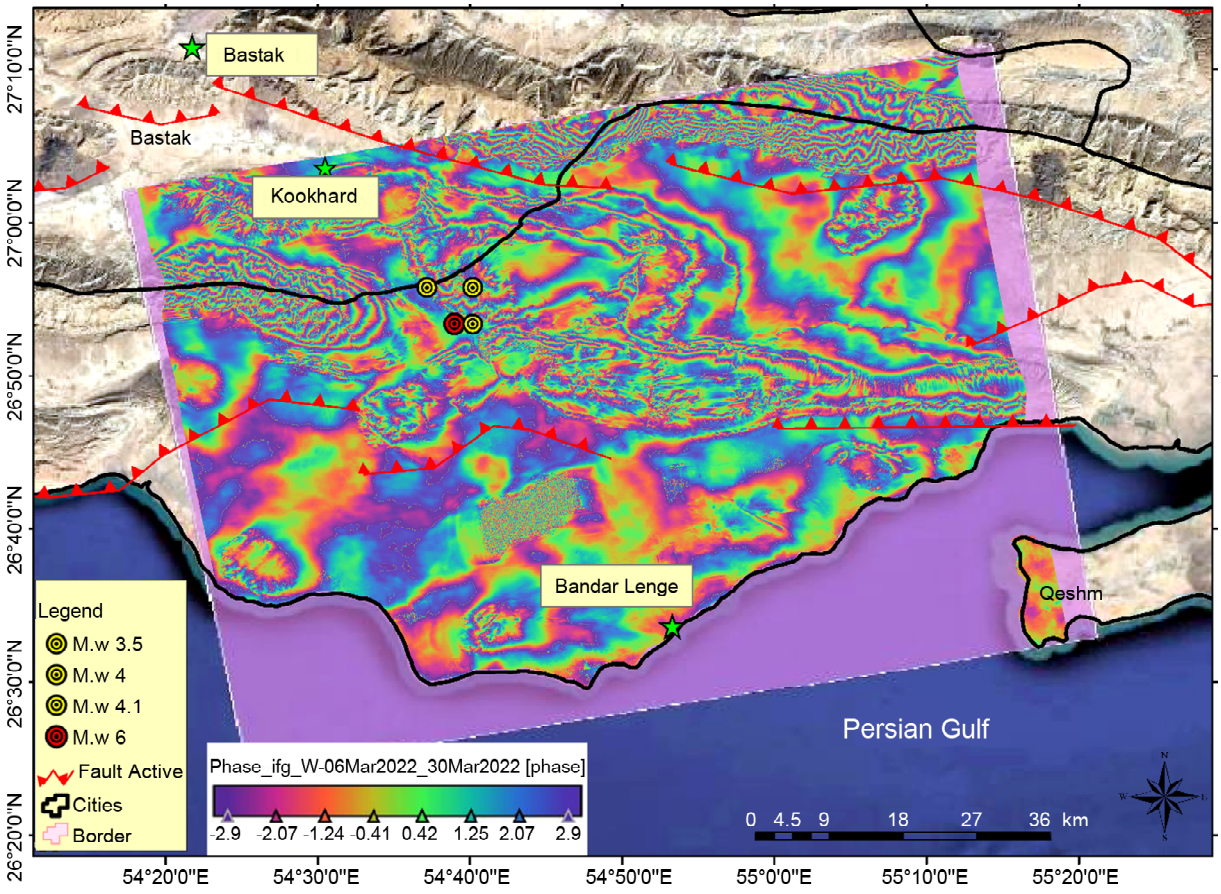

Figure 3. Image of seismic interference mapping caused by the 2022 March 16 Kookhord- Bastak earthquake (Mw6).

light blue and dark blue, the radar shift occurs. Generally, as can be seen from the map overlap image, the positive and negative fringes correspond to the linear trace of the faults in the area. Particularly, around the main epicenter of the earthquake can be seen fringes according to the fault trend (Figure 3).

4.1. Surface Displacement Map

After preparing the interference map from the area by applying filtering, possible errors such as speckle error and noise were removed from the image. Since the phase information is a 2π scale mapping interference, there is an ambiguous problem in calculating the correct number of phase cycles, which must be added to the phase observations in order to obtain the distances.

This ambiguity solution is known as phase ambiguity resolution. The process of retrieving ambiguous and correct phase values from a two-dimensional set of phase values in the range $(-\pi, \pi)$ is called two-dimensional phase recovery.

Finally, by performing the filter and resolving the phase ambiguity, a displacement map caused by the earthquake was prepared (Figure 4). As can be seen, not only the displacement was occurred around the earthquake epicenter, but also it has affected the faults around the epicenter and has caused changes in these areas.

According to the results, the maximum amount of the displacement is 19 cm, which is observed in the form of subsidence and in the red color on the map (Figure 4). Also, the amount of uplift after the earthquake is 14 cm shown in blue color on the map (Figure 4). It is mostly in the north-eastern part of the study area and corresponds with the trend of the faults.

5. Conclusion

The use of the satellite remote sensing in the Zagros mountain range can be a good way to studying the land surface deformation of an earthquake due to its extensive coverage and timeliness (appropriate temporal resolution). In this research, the displacements due to landslides in Koukhard-Bastak area has been investigated

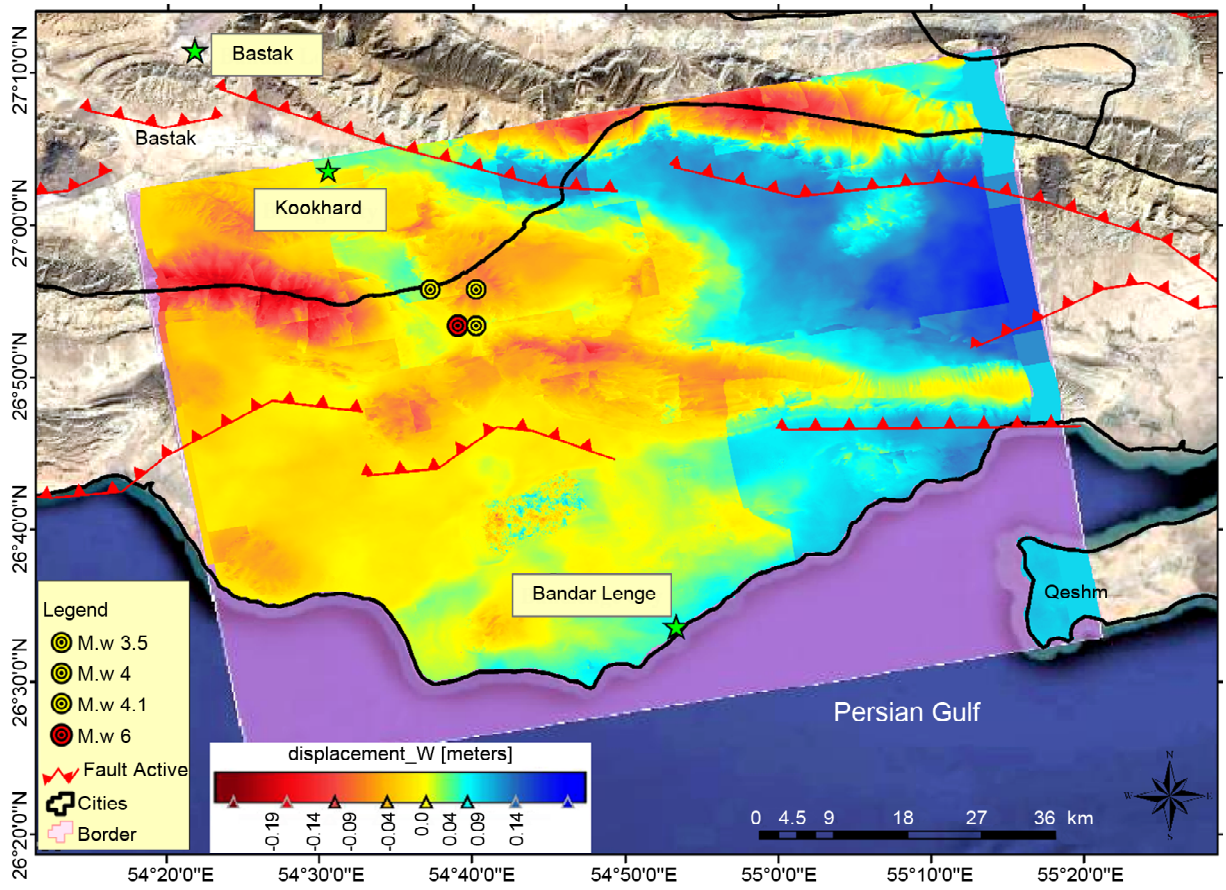

Figure 4. The final map of the displacements resulted of the March 16, 2022 Kookhord-Bastak earthquake (Mw6).

and determined with using radar interferometry method.

Evaluation of the results from the radar interferometry method, which providing accurate leveling, showed that the wide spatial coverage technique and the desired time have a high spatial accuracy for the detection of displacement vectors in the area.

The amount of ground displacement resulted of the earthquake in the Kookhord-Bastak area has been investigated by processing the Sentinel 1 satellite images. The results show that due to the presence of fault around the epicenter, the displacement caused by the earthquake is not only specific to that fault, but also affected the other faults around the epicenter.

The displacements map shows that a 19 cm displacement in the form of subsidence has been achieved in the western and northern parts of the area, while ~14 cm uplift is visible in the northeastern part of the area.

References

1. BNPB (2021) Indeks Risiko Bencana Indonesia (IRBI) Tahun 2020. In Badan Nasional Penanggulangan Bencana. Retrieved from https: //inarisk.bnpb.go.id/pdf/BUKU IRBI 2020 KP.pdf.

2. Rashidi, A. and Derakhshani, R. (2022) Strain and moment rates from GPS and seismological data in Northern Iran: implications for an evaluation of stress trajectories and probabilistic fault rupture hazard. *Remote Sensing*, **14**, 2219, https://doi.org/10.3390/rs14092219.

3. Al-Taie, A.J. and Albusoda, B.S. (2019) Earthquake hazard on Iraqi soil: Halabjah earthquake as a case study. *Geodesy and Geodynamics*, **10**(3), 196-204.

4. Pan, S.T., Cheng, Y.Y., and Lin, C.H. (2019) Extrication time and earthquake-related mortality in the 2016 Taiwan earthquake. *Journal of the Formosan Medical Association*, **118**(11), 1504-1514.

5. Roy, T. and Matsagar, V. (2020) Probabilistic assessment of steel buildings installed with passive control devices under multi-hazard scenario of earthquake and wind. *Structure and Infrastructure Engineering*, **85**(1), 1-17.

6. Yousuf, M., Bukhari, S.K., Bhat, G.R., and Ali, A. (2020) Understanding and managing earthquake hazard visa viz disaster mitigation strategies in Kashmir valley, NW Himalaya. *Progress in Disaster Science*, **5**(1), 1-11.

7. Rashidi, A., Kianimehr, H., Yamini-Fard, F., Tatar, M., and Zafarani, H. (2022) Present stress map and deformation distribution in the NE Lut Block, Eastern Iran: insights from seismic and geodetic atrain and moment rates. *Pure Appl. Geophys.*, **179**, 1887-1917, https:// doi.org/10.1007/s00024-022-03015-x.

8. Amarjargal, S., Kato, T., and Furuya, M. (2013) Surface deformations from moderate-sized earthquakes in Mongolia observed by InSAR. *Earth, Planets and Space*, **65**(7), 713-723.

9. Burgmann, R., Rosen, P., and Fielding, E. (2000) Synthetic Aperture Radar interferometry to measure Earth's surface topography and its deformation. *Annu. Rev. Earth. Planet. Sci.*, **28**, 169-212.

10. Taymaz, T., Wright, T.J., Yolsal, S., Tan, O., Fielding, E., and Seyitoglu, G. (2007) Source characteristics of the 6 June 2000 OrtaeCankiri (central Turkey) earthquake: a synthesis of seismological, geological and geodetic (InSAR) observations, and internal deformation of the Anatolian plate. *Geological Society, London, Special Publications*, **291**(1), 259-290.

11. Simons, M., Fialko, Y., and Rivera, L. (2002) Coseismic deformation from the 1999 Mw 7.1 Hector Mine, California earthquake as inferred from InSAR and GPS observations. *Bull. Seismol. Soc. Am.*, **92**, 1390-1402.

12. Qu, C., Zuo, R., Shan, X., Hu, J-C., and Zhang, G. (2017) Coseismic deformation of the 2016 Taiwan Mw6.3 earthquake using InSAR data and source slip inversion. *Journal of Asian Earth Sciences*, doi: http:// dx.doi.org/10.1016/ j.jseaes.2017.08.027.

13. Wright, T.J., Parsons, B.E., Jackson, J.A., Haynes, M., Fielding, E.J., England, P.C., and Clarke, P.J. (1999) Source parameters of the 1

October 1995 Dinar (Turkey) earthquake from SAR interferometry and seismic body wave modeling. *Earth Planet. Sci. Lett.*, **172**, 23-37.

14. Bardi, F., Raspini, F., Frodella, W., Lombardi, L., Nocentini, M., Gigli, G., Morelli, S., Corsini, A., and Casagli, N. (2017) Monitoring the rapid-moving reactivation of earth flows by means of GB-InSAR: The April 2013 capriglio landslide (Northern Appennines, Italy). *Remote Sensing*, **9**(2), 165.

15. Lombardi, L., Nocentini, M., Frodella, W., Nolesini, T., Bardi, F., Intrieri, E., Carlà, T., Solari, L., Dotta, G., Ferrigno, F., and Casagli, N. (2016) The Calatabiano landslide (Southern Italy): preliminary GB-InSAR monitoring data and remote 3D mapping. *Landslides*, **76**, 1-18.

16. Gabriel, A.K., Goldstein, R.M., and Zebker, H.A. (1989) Mapping small elevation changes over large areas: Differential radar interferometry. *J. Geophys. Res.*, **94**(B7), 9183-9191.

17. Livio, F., Serva, L., and Gürpinar, A. (2017) Locating distributed faulting: Contributions from InSAR imaging to probabilistic fault displacement hazard analysis (PFDHA). *Quaternary International*, **451**, 223-233.

18. Massonnet, D. and Feigl, K.L. (1998) Radar interferometry and its application to changes in the Earth's surface. *Rev. Geophys.*, **36**, 441-500.

19. Nakamura, T., Suzuki, S., Matsushima, T., Ito, Y., Hosseini, S.K., Gandomi, A.J., Sadeghi, H., Maleki, M., and Aghda, S.M.F. (2004) Source fault structure of the 2003 Bam earthquake, southeastern Iran, inferred from the aftershock distribution and its relation to the heavily damaged area: existence of the Arg-e-Bam fault proposed. Website: http://www.gaea.kyushuu.ac.jp/research/iran2004/paper/GRL2004.html.

20. Stramondo, S.M., Moro, Tolomei, C., Cinti, F.R., and Doumaz, F. (2005) InSAR surface displacement field and fault modeling for the Bam earthquake (southeastern Iran). *Journal of Geodynamics*, **40**(23), 347-353.

21. Cigna, F., Osmanoglu, B., Cano, E., Dixon, T., Olivera, J., Garduno-Monroy, V., and DeMets, C. (2012) Radar interferometry: A case study in morelia, Mexico. *Remote Sensing of Environment*, **25**(3), 146-161.

22. Kaneko, Y., Fialko, Y., Sandwell, D.T., Tong, X., and Furuya, M. (2013), Interseismic deformation and creepalong the central section of the North Anatolian Fault (Turkey): InSAR observations and implications for rate-and-statefriction properties. *J. Geophys. Res. Solid Earth*, **118**, 316-331, doi:10.1029/2012JB009661.

23. Feng, W., Lindsey, E., Barbot, S., Samsonov, S., Dai, K., Li, P., Li, Z., Almeida, R., Chen, J., and Xu, X. (2017) Source characteristics of the 2015 Mw 7.8 Gorkha (Nepal) earthquake and its MW 7.2 aftershock from space geodesy. *Tectonophysics*, 712-713C, 747-758.

24. Mohammadhasani, M., Kermani, B.S.S., Jameel, M., and Hakim Seyed, J.S. (2022) Estimation of land subsidence hazard using interferometry of satellite radar images. *Proceedings of the Institution of Civil Engineers - Forensic Engineering*, 0 0:0, 1-8.

25. Kandregula, R.D., Kothyari, G.C., Swamy, K.V., Taloor, A.K., Lakhote, A., and Chauhan, G. (2021) Estimation of regional surface deformation post the 2001 Bhuj earthquake in the Kachchh region, Western India using RADAR interferometry. *Geocarto International Journal*, **37**, https://doi.org/10.1080/10106049.2021.1899299.

26. Syafriani, D., Fikri, S., and Guvil, Q. (2022) Monitoring of land surface change in padang city using dinsar sentinel-1a method. *Journal of Applied Gespatial Information*, **6**(2), 615-619.

27. Hessami, K., Mobayyen, F., and Tabassi, H. (2013) *The Map of Active Faults of Iran*. International Institute of Earthquake Engineering and Seismology: Tehran, Iran.